eScience 3 (2023) 100133

Contents lists available at ScienceDirect

eScience

journal homepage: www.keaipublishing.com/en/journals/escience

Review

Conductive MOFs for electrocatalysis and electrochemical sensor

Kang-Kai Liu [a,1], Zheng Meng [b,1], Yu Fang [a,c,*], Hai-Long Jiang [b,*]

[a] State Key Laboratory for Chemo/Bio-Sensing and Chemometrics, College of Chemistry and Chemical Engineering, Hunan University, Changsha, 410082, Hunan, China
[b] Department of Chemistry, University of Science and Technology of China, Hefei, Anhui, 230026, China
[c] Innovation Institute of Industrial Design and Machine Intelligence Quanzhou-Hunan University, Quanzhou, 362801, Fujian, China

HIGHLIGHTS

- Electrocatalysis and electrochemical sensing with conductive MOFs are introduced.
- The "structure–property relationship" of conductive MOFs is summarized.
- Advances in using conductive MOFs for catalysis and sensing are discussed.
- Future perspectives on designing framework-based electrocatalysts and sensors in different dimensions are presented.

GRAPHICAL ABSTRACT

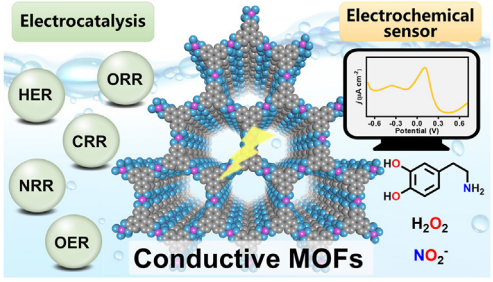

ARTICLE INFO

Keywords:
Metal-organic framework
Electrocatalysis
Electrochemical sensor
Conductive
Two-dimensional

ABSTRACT

Two-dimensional conductive metal–organic frameworks (2D-cMOFs) are a class of 2D layered MOFs with excellent electrical conductivity and other electronic properties. In recent years, their porous structure and dense active sites have been widely used in electrocatalysis and electrochemical sensing. The large electron delocalization domains generated by an extended π-conjugated framework through the covalent bonding between metal and organic ligand endow them with unique high conductivity. Yet despite a few promising applications, current research rarely addresses their "structure–property relationship." This review discusses the rational design of 2D-cMOFs with extraordinary electrochemical performance. We introduce several representative 2D-cMOFs and describe their applications, focusing on electrochemical catalysis and small molecule detection. By correlating the performance of the current materials in these applications and the corresponding mechanisms, we aim to uncover the key structural features that lead to their engineered properties and functions.

1. Introduction

With rapid human development, the world is now facing two major problems: the fossil fuel shortage and the pollution generated by fossil fuel combustion. On the one hand, non-renewable fossil fuel resources are rapidly being depleted; on the other hand, their combustion continues to create atmospheric pollution that causes global warming. The advancement of green, renewable energy systems is therefore essential for human beings and the planet. Among various techniques, electrochemical systems are very promising, as they are capable of precisely converting chemical energy into electrical energy through mild reactions at the electrode surface [1]. Since the electrochemical process does not require combustion, it has a higher theoretical thermodynamic efficiency. In addition, the process only generates water or economically useful

* Corresponding author.
E-mail addresses: yu.fang@hnu.edu.cn (Y. Fang), jianglab@ustc.edu.cn (H.-L. Jiang).
[1] Contributed equally.

https://doi.org/10.1016/j.esci.2023.100133
Received 28 November 2022; Received in revised form 14 February 2023; Accepted 5 April 2023
Available online 11 April 2023

products, without releasing pollutants. Thus, a variety of electrochemical systems, such as hydrolysis cells, are already part of our daily life [2].

The common electrochemical system usually contains water-splitting reactions, CO_2 reduction, and small molecule detection. (1) To generate renewable energy during the electrochemical process, the hydrogen evolution reaction (HER), oxygen evolution reaction (OER), and oxygen reduction reaction (ORR) have been developed [3,4]. They are the core reactions in electrocatalysis and have been thoroughly studied. The HER utilizes water as the substrate and converts it to hydrogen gas, the ultimate clean energy [5]. The OER and ORR can provide combustion resources or be incorporated into fuel battery systems. (2) To reduce greenhouse gases, including CO_2 and N_2, electrocatalysts can be used to convert them into alcohols or alkanes [6]. These reactions usually are conducted in mild, low-energy-demanding conditions. (3) To detect potential pollutants, drugs, and other small molecules, electrochemical systems are applied to capture electrical signals. In the presence of external stimuli, electrocatalysts convert small substrates into products, simultaneously generating electrical signals [7,8]. This method is widely used in industrial processes, pharmaceuticals, and environmental monitoring because it can be done online and is fast, sensitive, and inexpensive [9]. Hence, there is high demand for well-designed high-performance electrocatalysts.

Using porous materials to immobilize noble metals as electrocatalysts is a well-documented approach [10]. However, the low reserves and high prices of precious metals are constraints on the large-scale commercial production of these electrocatalysts, so cost-effective alternatives with high activity and stability are much needed. Since their discovery in the 1990s, porous nanomaterials have received increasing attention from scientists in many research fields, including medicine, chemistry, physics, and especially nanotechnology [11–13]. Metal–organic frameworks (MOFs) are long-range ordered framework structures composed of organic ligand units and inexpensive metal nodes [14]. MOFs with rich porosity and tunable active sites are applied in batteries, supercapacitors, electrocatalysis, and electrochemical sensors [15–18]. Most of these applications rely on the open redox sites of MOFs. However, during the actual reactions, their performance is severely constrained by high activation potential barriers, leading to high overpotentials that hinder efficiency and conversion, so inducing low-energy intermediates in MOF electrocatalysts is crucial to improving their performance [19]. In addition, the selectivity and sensitivity of electrochemical sensors for small molecules are largely dependent on the conductivity and redox sites of their electrode materials.

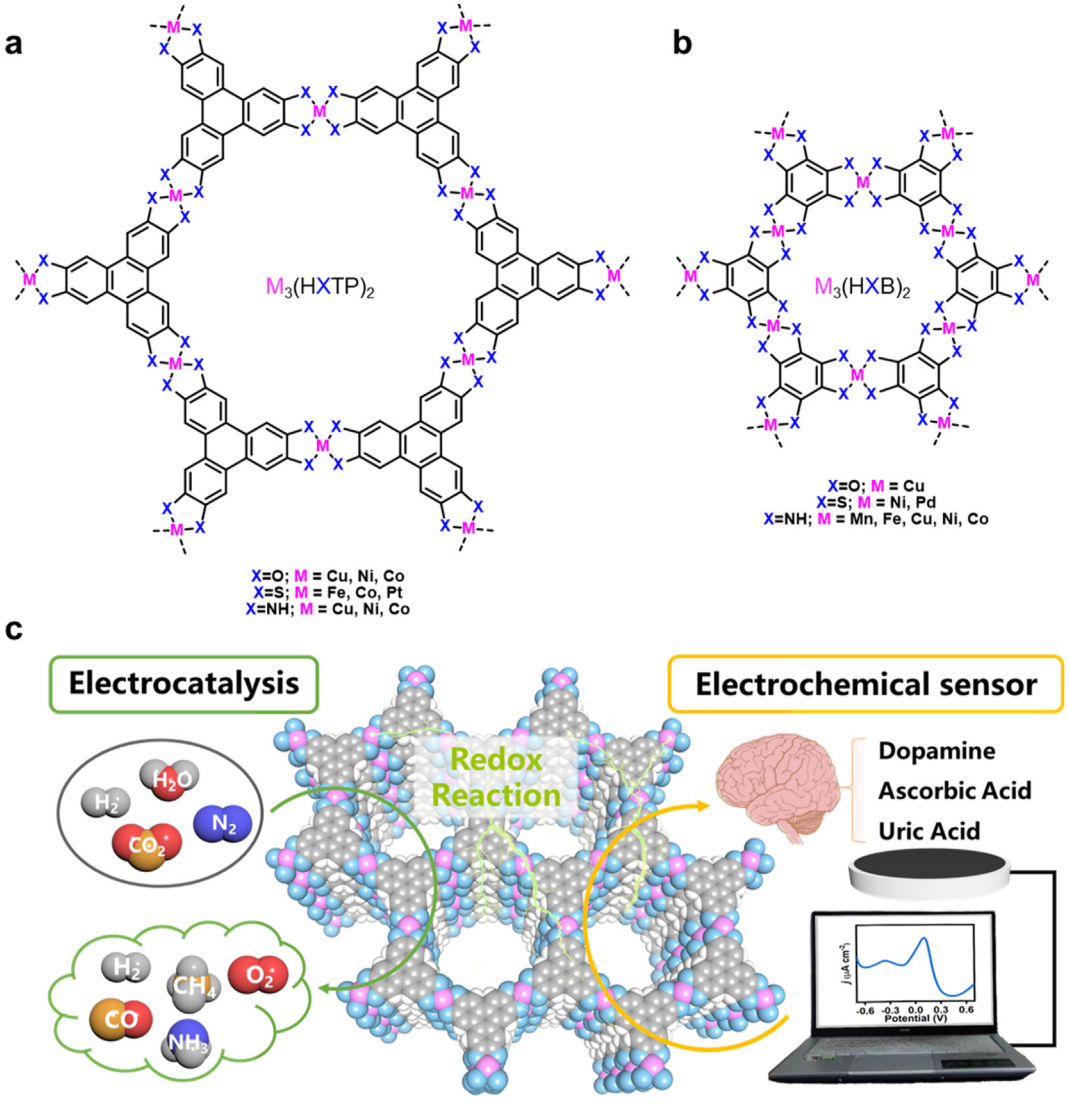

Fig. 1. Diagrams showing the structures of 2D-cMOFs conjugated with either (a) HXTP or (b) HXB. (c) Schematic illustration of 2D-cMOFs in the redox reaction mechanism for electrocatalysis and electrochemical sensing.

To improve the electrical conductivity of MOF-based materials, a pyrolytic annealing method is usually used to obtain MOF-derived metal oxide carbon nanocomposites [20]. Although this method improves their electrical conductivity, it dramatically reduces the specific surface area and the intrinsic crystallinity of the MOFs. In addition, this process may also increase the materials' hydrophobicity, which is not favorable for the reaction in aqueous electrolytes [21]. Two-dimensional conductive metal–organic frameworks (2D-cMOFs) are a class of 2D layered MOFs with good electrical conductivity through tightly stacked π-π interactions. 2D-cMOFs usually contain highly symmetrical conjugated organic nuclei as redox non-innocent ligands and transition metals as nodes (Fig. 1). As ordered microporous materials, they show extremely high electrical conductivity [22,23]. There tends to be a strong electron delocalization domain within the 2D layer that accounts for the high conductivity, which is generated by the formation of extended π-conjugated frameworks through covalent bonds between the metal and the ligand: (1) MOFs contain catecholate linkers that are highly oxidizable, resulting in organic radicals; (2) the radicals are locally delocalized and stabilized, thanks to full conjugation within the linker; (3) as the linker orbitals match the metal frontier orbitals, the conjugated system extends throughout the entire layer; in addition, the extended conjugation of the π-systems depends on the material's overall geometry because coplanar linkers create flat 2D layers [24]. During this review, we discuss and summarize the applications of 2D-cMOFs in electrochemical catalysis and sensors (Table 1) in which 2D-cMOF-mediated redox events occur at the surface of the MOFs at certain potentials (Fig. 1c).

As an intrinsic property of crystalline materials, the topology of 2D-cMOFs has an important influence on their electrochemical properties. That pore size can be designed by adjusting the ligand size implies that a larger pore facilitates mass transfer. Meanwhile, the metal centers involved in coordination affect the layer spacing of the π-conjugated structure, which directly impacts electron transfer and active site utilization [25,26]. 2D-cMOFs are unsaturated and coordinated, with defects and catalytic sites, so their stability in electrochemical processes is determined by their tolerance to degradation and competition. Stability comes from the strength of the ligand bonds, which can be roughly evaluated based on the hard–soft acid–base theory for the aqueous environment where the reaction takes place. The surface of 2D-cMOFs attracts ions of opposite charge at a given voltage, and then the metal sites can be reduced or oxidized at a certain potential. This change in metal valence affects the hardness and coordination conditions of the metal nodes. Since the electrocatalytic process takes place on the surface/interface, defects or coordination of unsaturated sites on 2D-cMOFs can promote catalytic activity [27,28]. Tunable components provide platforms for modulating the electronic structure and adsorption capacity of the active sites. These electrochemical properties are superior to those of conventional MOFs and reflect the significance of using 2D-cMOFs for the development of electrocatalysis. As the study of 2D-cMOFs in electrocatalysis and sensors is still in the initial stage, great opportunities lie ahead.

2. Electrocatalysis

2.1. HER

Water electrolysis is the simplest and most effective method to convert renewable resources into hydrogen energy for storage. Recently, 2D-cMOFs exhibited better electrocatalysis than carbon nanotube-loaded molecular or heteroatom-doped graphene catalysts [29]. Nishihara's group obtained a π-conjugated nanosheet (Compound 1) by a liquid interface reaction with benzene hexathiol [30]. Compound 1 had semiconducting nickel bis(dithiolene) units (Fig. 2a) with thicknesses of a few microns and exhibited powerful charge delocalization domains between the metallodithiolene units in the mixed valent state through the phenylene junction. Despite its highly developed π-conjugation, the material had a very low conductivity at room temperature, 0.15 S cm^{-1}. In addition, Compound 1 showed reversible redox behavior, which is expected during catalytic cycles with many active sites.

Inspired by Ni-dithiolene as the active unit, Feng and co-workers developed a 2D-cMOF (Fig. 2b) with a Ni-dithiolene active unit (Compound 2) composed of 1,2,5,6,9,10-triphenylene hexathiol (THT) and Ni ion [31]. This overcame the disadvantage of previous interfacial methods that only yielded nanosheets with a small lateral dimension of 5 μm. In contrast, Compound 2 had lateral dimensions in the square millimeters range and thicknesses of 0.7–0.9 nm, and it could be completely transferred to many different types of substrates. Notably, the well-distributed Ni-dithiolene fraction in Compound 2 was fully exposed, leading to an efficient HER of 80.5 mV dec^{-1}. Following this study, they synthesized a

Table 1
The performance of 2D-cMOFs for different electrochemical catalysis and sensors.

Reaction	Material	Ligand	Abbreviation	Ref.
HER	Ni-BHT	BHT	Compound 1	[30]
	Ni-THT	THT	Compound 2	[31]
	NiAT	1, 3, 5-triaminobenzene-2, 4,	Compound 3	[33]
	NiIT	6-trithiol	Compound 4	
	$Ni_3(Ni_3{\cdot}HAHATN)_2$	HATN	Compound 5	[35]
	$Ni_3(Co_3{\cdot}HAHATN)_2$		Compound 6	
	$Ni_3(Cu_3{\cdot}HAHATN)_2$		Compound 7	
	$Cu_3(Cu_3{\cdot}HAHATN)_2$		Compound 8	
OER	NiPc-MOF	$NiPc\text{-}NH_2$	Compound 9	[38]
	$NiPc\text{-}NiFe_{0.09}$	NiPc-OH	Compound 10	[39,40]
	NiPc-Ni		Compound 11	
	Co–HAB	HAB	Compound 12	[41]
ORR	$Ni_3(HITP)_2$	HITP	Compound 13	[43]
	Ni-CAT	HHTP	Compound 14	[46]
	Co-CAT		Compound 15	
	$Co_{0.27}Ni_{0.73}$-CAT		Compound 16	
CRR	Cu-DBC	8OH-DBC	Compound 17	[53]
	Cu-HHTP	HHTP	Compound 18	
NRR	$Co_3(HHTP)_2$	HHTP	Compound 15	[59]
Electrochemical sensors for	$Ni_3(HITP)_2$	HITP	Compound 13	[62]
inorganic probes and neurochemicals	$Cu_3(HITP)_2$	HHTP	Compound 19	
	$Ni_3(HHTP)_2$		Compound 14	
	$Cu_3(HHTP)_2$		Compound 18	
Electrochemical sensor for H_2O_2	Cu-BHT	BHT	Compound 20	[67]
Electrochemical sensor for nitrite	NiPc-MOF	$NiPc\text{-}NH_2$	Compound 9	[70]

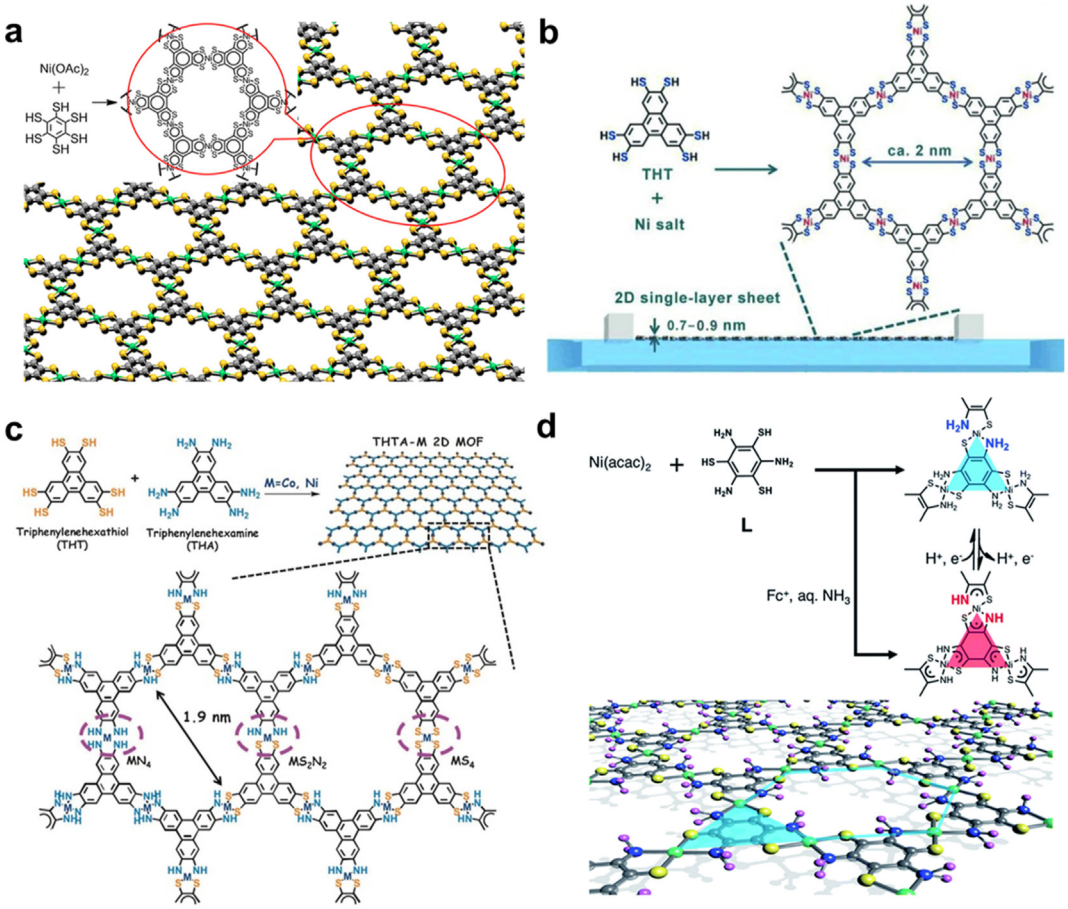

Fig. 2. (a) An illustration of the Compound 1 structure. Reprinted with permission from Ref. [30]. Copyright 2013, American Chemical Society. (b) The synthesis of Compound 2. Reprinted with permission from Ref. [31]. Copyright 2015, Wiley-VCH. (c) Metal dithiolene-diamine coordination synthesis of THAT-M 2D MOFs containing three moieties. Reprinted with permission from Ref. [32]. Copyright 2017, Wiley-VCH. (d) Synthesis and molecular structures of Compound 3 and Compound 4. Reprinted with permission from Ref. [33]. Copyright 2017, Royal Society of Chemistry.

series of 2D-cMOF solid electrocatalysts with three active centers (Fig. 2c), using THT and 2,3,6,7,10,11-hexaiminotriphenylene (HITP) as ligands with Co and Ni as metal centers [32]. Elemental analysis and density functional theory (DFT) calculations indicated these 2D-cMOFs had definite active sites for electrocatalytic hydrogen production. The electrocatalytic activity of the above three active centers followed the order metal bis(dithiolene)-diimine > metal bis(diimine) > metal bis(-dithiolene), which provided a new idea for advancing 2D-cMOFs for electrocatalysis. After 400 CV cycles, the overpotential increased by only 10 mV (10 mA cm^{-2}), indicating that the material exhibited good electrochemical stability in acidic electrolytes.

Based on the good conductivity of Compound 1, Nishihara's team developed bis(aminothiolato)nickel (Compound 3), shown in Fig. 2d [33]. Compound 3 formed flat crystalline sheets stacked in a staggered arrangement with a Kagome lattice. The $2H^{+}$-$2e^{-}$ reaction allowed Compound 3 to be reversibly converted into bis(iminothiolato)nickel (Compound 4) nanosheets. Due to the difference in the energy band structure, Compound 3 became less conductive and Compound 4 became more conductive. In addition to having a high acid resistance and an onset overpotential of −0.15 V, Compound 3 exhibited a Tafel slope of 128 mV dec^{-1} in HER electrocatalysis. Results from 500 HER cycles indicated that NiAT is an efficient and durable electrocatalytic cathode material for hydrogen production from water under acidic conditions.

Researchers are gradually finding 2D-cMOFs composed of N-conjugated ligands. In particular, excellent electrical conductivity is achieved by their metal bonding and M–N_4 conjugated organic ligands. Although these conducting MOFs seem to have potential applications for electrocatalysis due to their extraordinary structures, they are still not as electrically active as for practical applications. Results have shown that the metal ions of M–N_4 exhibit little effective catalytic activity, as the bonds remain in the original oxidation state during electrocatalysis [34]. Hence, it is crucial to design conjugated organic ligands equipped with additional coordination sites. Hexaazatriphenylene (HATN) provides extra sites for binding highly active metal centers for electrocatalysis. Chen and co-workers used HATN with a bidentate tertiary amine coordinated with Ni ion to form Compound 5 nanosheets (Fig. 3) with a bidentate coordination part [35]. The results exhibited a small overpotential of 115 mV at 10 mA cm^{-1}, and a low Tafel slope (45.6 mV dec^{-1}). Compound 5 had a current density of 21.2 mA cm^{-2} at −0.15 V, around four times higher than Compound 13. Compared with the series of Compound 6, Compound 7, and Compound 8, $M2_3$ $(M1_3{\cdot}HAHATN)_2$ nanosheets had excellent electron transfer conductivity. The metal ion fraction introduced in M1-N_2 exhibited higher unsaturation than conventional M2-N_4. DFT calculations predicted that the main activity center of the HER in $M2_3$ $(M1_3{\cdot}HAHATN)_2$ is the M1-N_2 part rather than the M2-N_4 bond. After 1000 cycles, crystalline data and morphology indicated that the rigid conjugated coordination structure gave Compound 5 excellent durability in HER processes.

As the HER is one of the most important semi-reactions of water electrolysis, there are higher requirements for materials' inherent electron transfer ability. The π-π stacking structure of a transition metal as a node component gives 2D-cMOFs unique advantages in the HER, leading to lower overpotential and better catalytic activity than a noble metal catalyst.

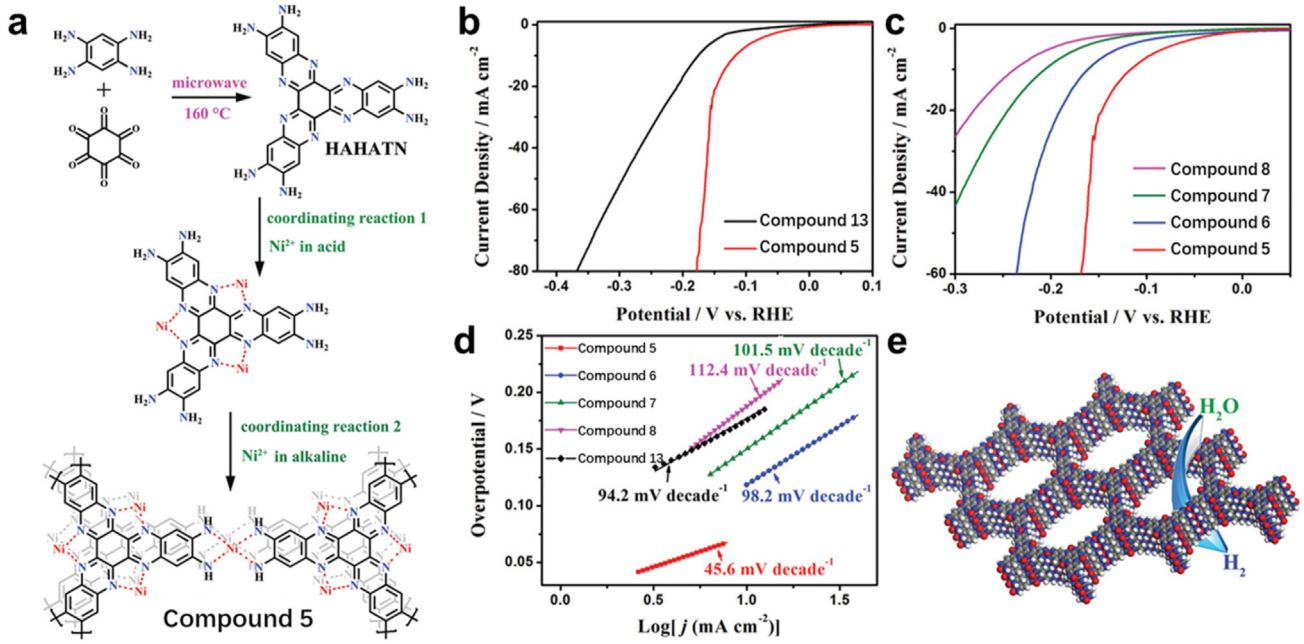

Fig. 3. (a) Synthetic diagram of Compound 5 MOFs. (b) HER polarization curves of Compound 13 and Compound 5. (c) Polarization curves of the various $M2_3(M1_3{\cdot}HAHATN)_2$ samples and (d) the corresponding Tafel plots. (e) Electrocatalytic scheme of Compound 5 nanosheets. Reprinted with permission from Ref. [35]. Copyright 2020, Wiley-VCH.

2.2. OER

Aside from the HER, which occurs at the cathode, another important half-reaction for brine electrolysis is the OER, which takes place at the anode. The OER is a kinetically slow process involving 4-electron/proton transfer, which has different reaction mechanisms under different pH conditions [36,37]. The Du group synthesized an innovative nickel 2D-cMOF (Compound 9) using 2,3,9,10,16,17,23,24-octaamino-phthalocyaninato nickel (II) (NiPc-NH_2) as a ligand (Fig. 4a) [38]. The NiPc part acted as not only a linking unit but also an electrocatalytic active site with

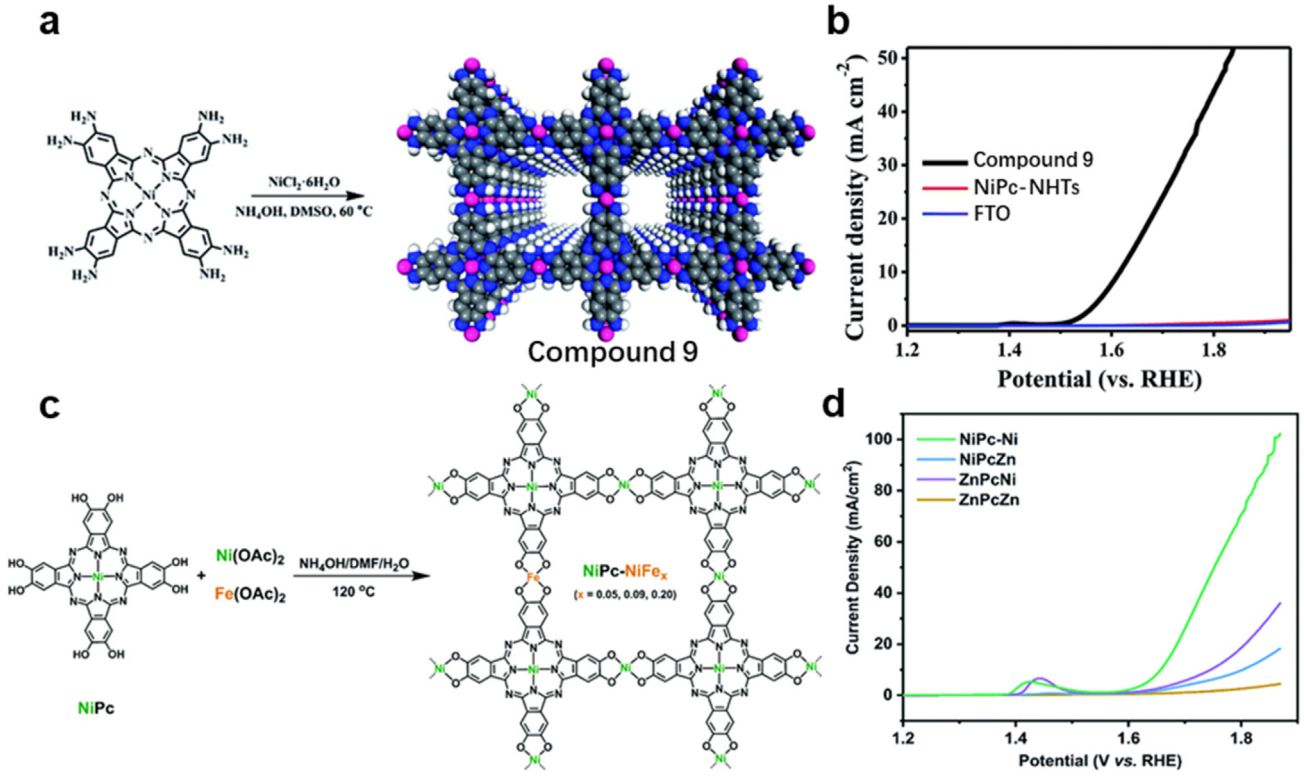

Fig. 4. (a) Synthetic strategy and structure of Compound 9. (b) LSV curves of NiPc–MOF, NiPc–NHTs, and FTO at 10 mV s^{-1} for the OER. Reprinted with permission from Ref. [38]. Copyright 2018, Royal Society of Chemistry. (c) Chemical synthesis procedure for NiPc-$NiFe_x$ MOFs. (d) LSV curves using NiPc-$NiFe_x$ MOFs as catalysts for the OER. Reprinted with permission from Ref. [39]. Copyright 2021, Royal Society of Chemistry.

extremely low onset potential (< 1.48 V) and overpotential (< 0.25 V) and high-quality activity (883.3 A g^{-1}) for the OER at 350 mV (Fig. 4b). It also provided a high Faradaic efficiency (FE) (> 94% in 6000 s), showing excellent catalytic durability during long-term chronopotentiometry experimentation and a featureless UV–vis curve. They found that the phthalocyanine moiety can adopt various kinds of active sites.

Later on, the Song group modified the electronic structure of 2D-cMOFs by using phthalocyanine as a linker and additional metal sites as building blocks (Fig. 4c) [39]. By replacing Ni–O_4 in Compound 11 with Fe–O_4, 2D-cMOFs (NiPc-$NiFe_x$) were cost-effectively constructed. Electrochemical tests confirmed that Compound 10 had a small overpotential of 300 mV (at 10 mA cm^{-2}), a low Tafel slope of 55 mV dec^{-1}, and a remarkable TOF value of 1.943 s^{-1} ($\eta = 300$ mV) (Fig. 4d). The underlying activity of NiPc-NiFe was significantly enhanced by the electronic interactions between Ni–O_4 and Fe–O_4. To investigate the activity of Ni metal centers, the same research team characterized Compound 11 prepared by using nickel phthalocyanine, which resulted in a low onset overpotential of < 320 mV and a Tafel slope of 83 mV dec^{-1} [40]. This indicated that the electrostatic interactions of O_4–N_4 could enhance the OER activity. The stability of NiPc-Ni was measured using chronoamperometry testing and the Ni 2p XPS spectrum, which indicated good durability during the OER test. DFT calculation proved that electron modulation can be an effective method to design a bimetallic 2D-cMOF with excellent electrocatalytic reactivity. Not coincidentally, Fu and co-workers constructed ultrathin 2D-cMOFs nanosheets (Compound 12-NSs) by using hexaaminobenzene (HAB) as an organic junction (Fig. 5a) [41]. Owing to highly delocalized electrons and the strong π-d interaction of Co(II) with HAB, the conductivity of Co-HAB-NSs was 0.2 S cm^{-1}. Compound 12 displayed a uniform flower-like shape and a diameter of 500 nm (Figs. 5b and c). There was a significant difference between the Tafel slopes of Compounds 12-NP, 12-S, and 12-HNs compared with that of Compound 12, which caused poorer OER activity (Figs. 5d, e and f). Compound 12-NSs also possessed a lower overpotential (310 mV) and Tafel slope (56 mV dec^{-1}) through the agglomeration of nanoparticles.

As the OER involves a kinetically slow process of 4-electron/proton transfer, the structure of μ4-M greatly improves electron mobility. Through this strategy, 2D-cMOFs with high conductivity can exhibit excellent OER performance, which explains the electron transfer pathway in the interface reaction.

2.3. ORR

As an important reaction, the ORR is an irreversible process and has a sophisticated mechanism [42]. For oxygen and peroxide, the electrolyte should be stable. Furthermore, the overpotential should be lower than 1.23 V (vs. the reversible hydrogen electrode, RHE). Considering these factors, the Dincă group synthesized Compound 13 (Figs. 6a and b) using HITP [43]. Without post-synthesis treatment or modification, Compound 13 possessed a high conductivity of 40 S cm^{-1}. An onset potential (j = −50 μA cm^{-2}) of 0.82 V was obtained in an O_2 atmosphere by using Compound 13 films of 120 nm grown on glassy carbon rotating disk electrodes. The ORR activity of the material was 88% of the initial current density after 8 h. The results showed the same amount of Ni, demonstrating its excellent cycling stability. Compared to the theoretical Tafel slope of Compound 13 (−120 mV dec^{-1}), its experimental value was −128 mV dec^{-1}. Inductively coupled plasma mass spectrometry and atomic absorption spectrometry analysis of the film before and after electrolysis showed the same amount of Ni, indicating that no part of the catalyst was lost in the films during the catalytic process.

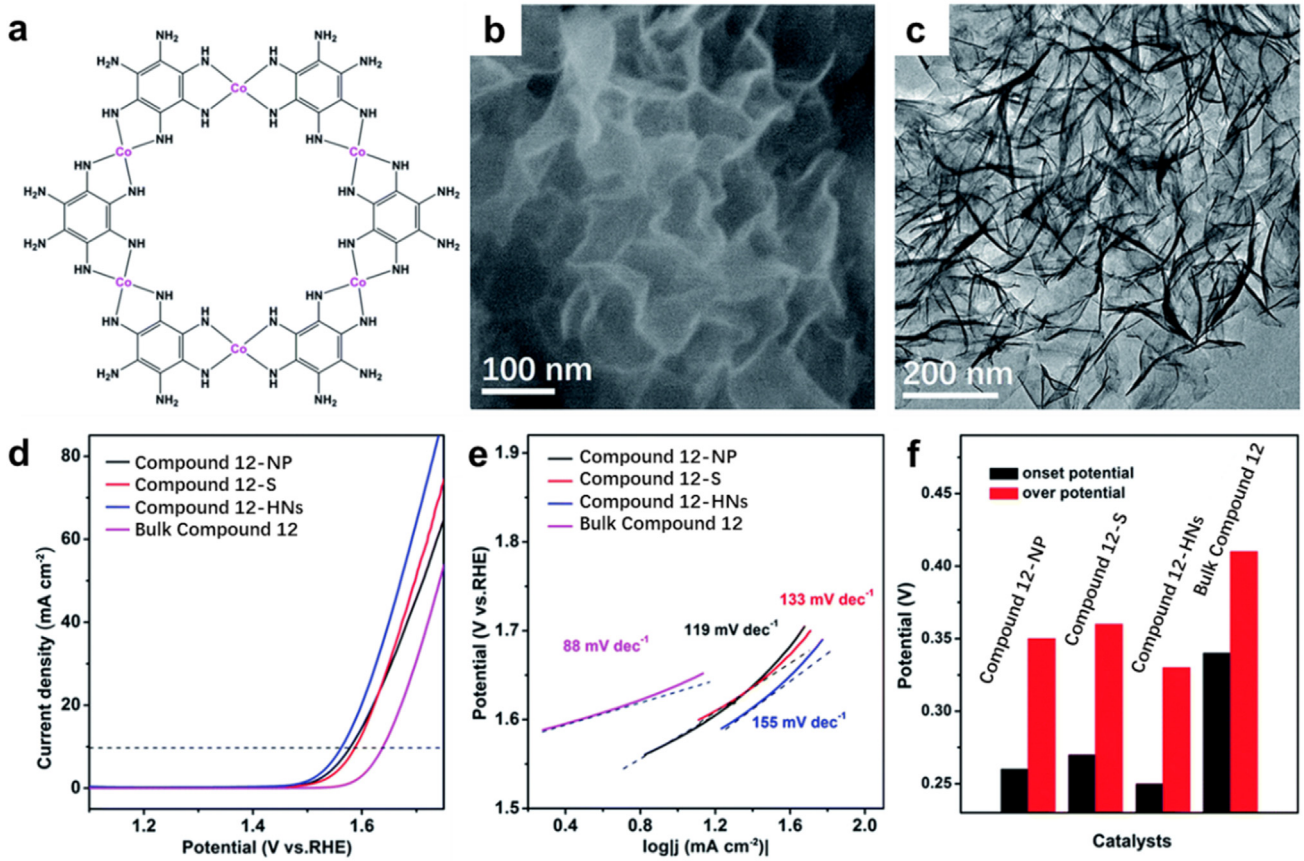

Fig. 5. (a) Chemical synthesis procedure for Co-HAB-NSs. (b) SEM and (c) TEM images of Compound 12. (d) LSV curves, (e) Tafel slopes, and (f) onset potential and overpotentials of Compound 12-NP, Compound 12-S, Compound 12-HNs, and bulk Compound 12. Reprinted with permission from Ref. [41]. Copyright 2020, Royal Society of Chemistry.

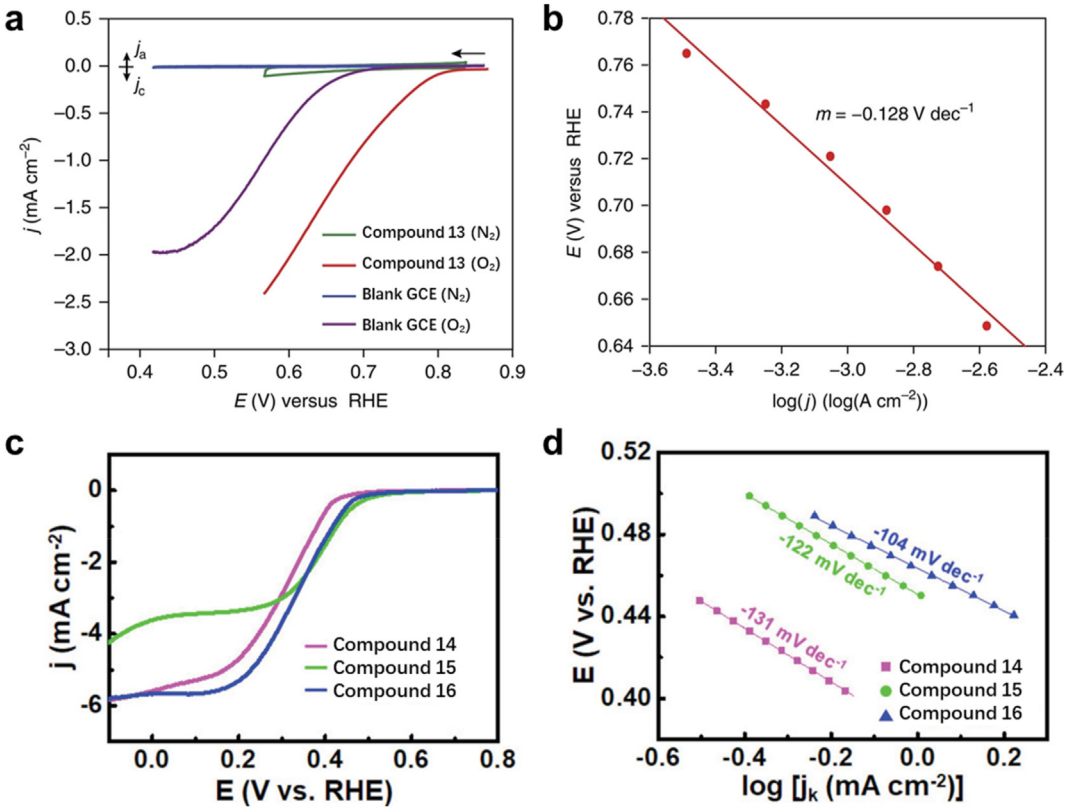

Fig. 6. (a) Polarization curves of Compound 13 and the blank GCE. (b) Tafel plot derived from the Koutecky–Levich plots for Compound 13-based ORR. Reprinted with permission from Ref. [43]. Copyright 2016, Nature. (c) LSV of Compound 15, Compound 14, and Compound 16. (d) Tafel plots and slopes for Compound 15, Compound 14, and Compound 16. Reprinted with permission from Ref. [46]. Copyright 2019, Wiley-VCH.

Although Compound 13 exhibited excellent ORR performance, its active site is still unclear. To better investigate catalytic activity, Omar M. Yaghi selected Compound 14 and Compound 15 (Figs. 6c and d), using 2,3,6,7,10,11-hexahydroxybenzophenol (HHTP) as the ligand [44,45]. Then, Hu's group systematically investigated the electrocatalytic ability of those two 2D-cMOFs. Both Compound 14 and Compound 15 had abundant nanopores and robust bimetallic doping [46]. Compared with either of these monometallic MOFs, bimetallic MOFs showed higher ORR activity by rationally regulating varied ratios of Co^{2+} and Ni^{2+}. Compound 16 retained a larger diffusion-limited current density ($j_{l@0.0\ v} = -5.68$ mA cm^{-2}) than Compound 15, and a higher onset potential (0.46 V vs. Compound 14). After 10,000 s, the Ni-CAT maintained 83% activity, and its EIS spectrum and PXRD patterns did not change significantly. In addition, this research demonstrated that a convenient ball milling method could be utilized to mass produce high-quality bimetallic MOFs with excellent ORR activity.

In summary, electrocatalysis of the oxygen reduction reaction is an important application of MOFs. A controllable bimetallic structure and uniform distribution of active sites are key features for 2D-cMOFs to deliver high ORR activity.

2.4. Other reduction reactions

Beyond the HER, OER, and ORR, other important reactions include the CO_2 reduction reaction (CRR) and the nitrogen reduction reaction (NRR). The CRR electrocatalytic is a green, efficient, and scalable technology with the potential to convert CO_2 while generating high-value chemicals, thereby relieving some of the current global energy crisis. Hence, developing the CRR is very important for this reason and to address environmental contamination problems [47]. 2D-cMOFs have made encouraging progress in early electrocatalytic CRR research to obtain CO (Feng's group and Mirica's group), C_2H_6 (Chen's group), and other chemicals [48–50]. Among the various CRR products, CH_4 is a particularly promising alternative to fossil fuel resources. However, the selectivity of the CRR to yield CH_4 is still at a very low level due to interference from the competing HER and multiple-electron transmission during the reaction process [51]. Cu-based electrocatalysts such as copper oxides, copper metal, and copper-containing materials are useful for facilitating the acquisition of hydrocarbon and alcohol products at appropriate FE. However, the difficulty of confirming the active site still hinders the selectivity of CRR electrocatalysts [52]. Lan's group investigated Compound 17, consisting of highly conjugated dibenzo-[g,p] chrysene-2,3,6,7,10,11,14,15-octanol (8OH-DBC) and Cu ion, for the CRR (Fig. 7a) [53]. The good electrical conductivity (1.2×10^{-2} S m^{-1}) of Compound 17 and Cu–O_4 sites facilitated a highly selective CRR-to-CH_4 process. The results indicated that the CH_4 FE was ~80% at −0.9 V, and the partial current density was −162.4 mA cm^{-2} relative to RHE. Compound 18 with Cu–O_4 sites was studied, as well as two other COFs containing the most extensively studied Cu–N_4 sites, metal porphyrins (Cu-TTCOF) and metal phthalocyanines (Cu–PPCOF). The FE of Compound 18 for CH_4 and C_2H_4 reached ~42.6% and ~40.9%, respectively (Fig. 7b). Although the selectivity for CH_4 was low, the compound still yielded hydrocarbons with a maximum FE of ~83.5%. The electrochemical activity and structural morphology of the materials before and after the reaction had not changed significantly, indicating the robustness of the M–O coordination bond. The products generated by Cu–PPCOF electrocatalysis were mainly H_2, with small amounts of CH_4 and CO. The activation process was more easily reduced to the low valent state on the Cu site. The presence of Cu–O_4 in Compound 17, rather than Cu-TTCOF and Cu–PPCOF, was favorable for the CRR.

Ammonia (NH_3) is a common product in the petroleum industry and an essential raw material, acting as a main basic precursor in the production of industrial nitrogen fertilizers, chemical fibers, explosives, and other chemical products [54]. Currently, the nitrogen reduction reaction

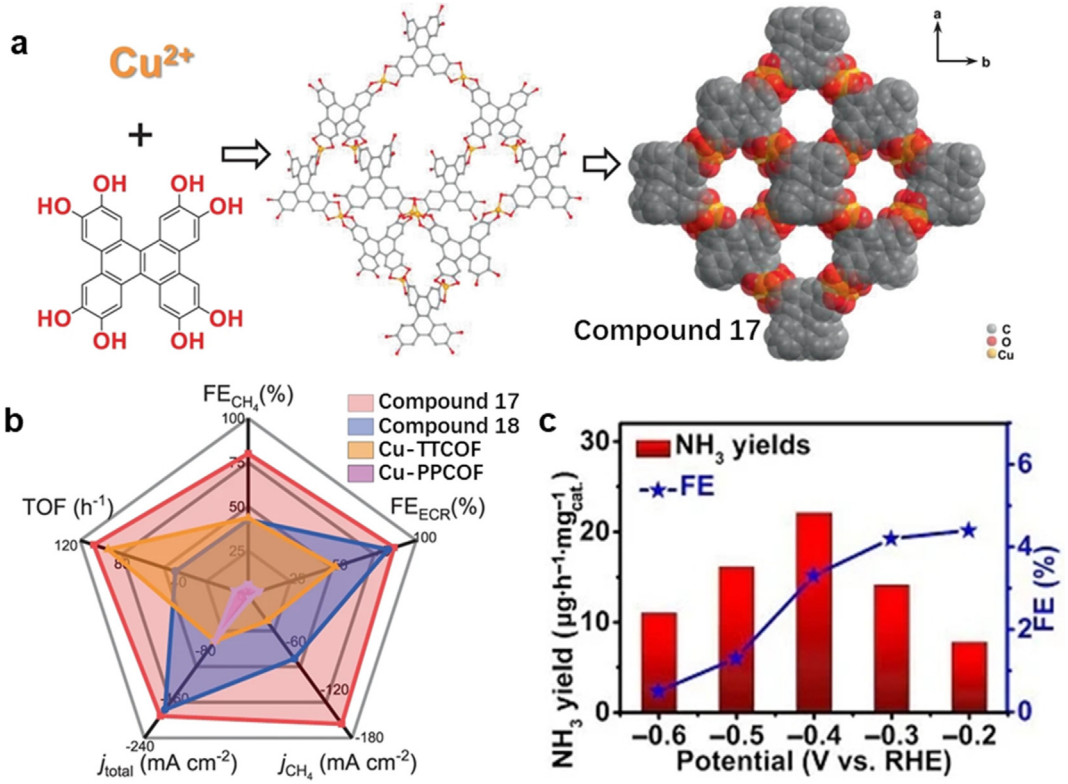

Fig. 7. (a) The synthesis and structure of Compound 17. (b) Overall ECR performance evaluation at −0.9 V *vs.* RHE. Reprinted with permission from Ref. [53]. Copyright 2021, Nature. (c) Corresponding NH_3 Compound 15/CP at various potentials. Reprinted with permission from Ref. [59]. Copyright 2020, Springer-Verlag.

(NRR) by the conventional Haber–Bosch process occurs under high temperature and pressure conditions using N_2 and H_2 in the presence of a catalyst such as iron or ruthenium [55,56]. Compared to photocatalytic reactions that utilize renewable energy conversion for the NRR, electrocatalysis has advantages: (1) elimination of fossil fuel consumption and CO_2 emissions; (2) easy modularization of the electrochemical plant; and (3) sustainable ammonia production [57]. The Sun group explored the effect of Mo-HAB on the NRR by DFT at the atomic level [58]. The results indicated that Mo-HAB exhibits strong N_2 adsorption capacity and weak adsorption of H_2O. In addition, its low overpotential (0.18 V) and high stability make it a highly selective NRR catalyst in ambient conditions. The 2D-cMOF Compound 15 is an efficient NRR electrocatalyst studied by Xuping Sun and co-workers (Fig. 7c) [59], whose experimental results showed that 3.34% FE at −0.40 V vs. RHE and very high NH_3 catalytic yields (22.14 μg h^{-1} mg^{-1}) were obtained in 0.5 M $LiClO_4$. In addition to the above properties, it is essential to assess electrocatalysts' stability and durability in practical applications to ensure sufficient working time at a certain potential. This is of great significance for their subsequent development and commercialization [60].

The advent of 2D-cMOFs has added more possibilities for MOFs in the field of electrocatalysis. The replaceable metal center and adjustable structure play a key role in the preparation of high-value-added electrocatalytic synthesis. Further, in the quest to understand the structure–activity relationship of traditional materials in the field of electrocatalysis, 2D-cMOFs have shown huge potential and achieved gratifying results.

3. Electrochemical sensors

3.1. Neurochemical

As electrode materials for electrochemical sensors, 2D-cMOFs have several significant advantages: (1) These materials are synthesized in one step by a simple hydrothermal method. Structural control and combinatorial modularity are easily achieved by adjusting the ligand and metal centers, and the redox electrocatalytic integrations are uniformly dispersed in the framework. (2) Permanently porous 2D-cMOFs can fully expose potential redox-active sites for electrochemical driving, which is essential to obtain the large current intensity required for enhancing the sensitivity of electrochemical sensors. (3) Their good conductivity allows 2D-cMOFs to be used directly as working electrodes in devices, without additional physicochemical modifications or the preparation of composites [61]. Overall, it is feasible to develop 2D-cMOFs into multifunctional integrated components for electroanalytical devices with remarkable chemical sensing capacity.

To investigate the performance of the most commonly used 2D-cMOFs in electrochemical sensors, Mirica's group designed 2D-cMOF-based electrode films containing Compound 13, Compound 14, Compound 19, and Compound 18 (Fig. 8a) [62]. The conductivities of the selected MOFs were characterized by 4-point probe in the range of 0.02–2 S m^{-1}. The design of this work depends on the proven electrocatalytic performance of metal centers for the redox-catalyzed conversion of neurochemical small molecules. Organic junctions or hydrogen bonds can interact intermolecularly with the target molecule. The inorganic probe is an essential detection molecule commonly used to assess the electrochemical sensing properties of materials. $FeCl_3$ and $K_3Fe(CN)_6$ are typically used as inner-domain probes with high sensitivity, while $Ru(NH_3)_6Cl_3$ is an outer-domain probe with typical insensitivity [63]. Therefore, $FeCl_3$, $K_3Fe(CN)_6$, and $Ru(NH_3)_6Cl_3$ were selected to analyze the electrochemical performance of the 2D-cMOFs. The results showed that the electroanalytical responses to the three inorganic probes were energetically affected by the surface chemistry, stacking morphology, and intrinsic conductivity of the 2D-cMOFs. Compound 13 showed the greatest change in k_0, with a maximum rate constant from $Ru(NH_3)_6Cl_3$ (6.41×10^{-3} cm s^{-1}), followed by $K_3Fe(CN)_6$ (4.44×10^{-3} cm s^{-1}) and $FeCl_3$ (9.05×10^{-3} cm s^{-1}) in the irreversible redox process. The materials all had the fastest k_0 for $Ru(NH_3)_6Cl_3$, probably because of its surface insensitivity, while the surface-sensitive probes had different k_0 ranges.

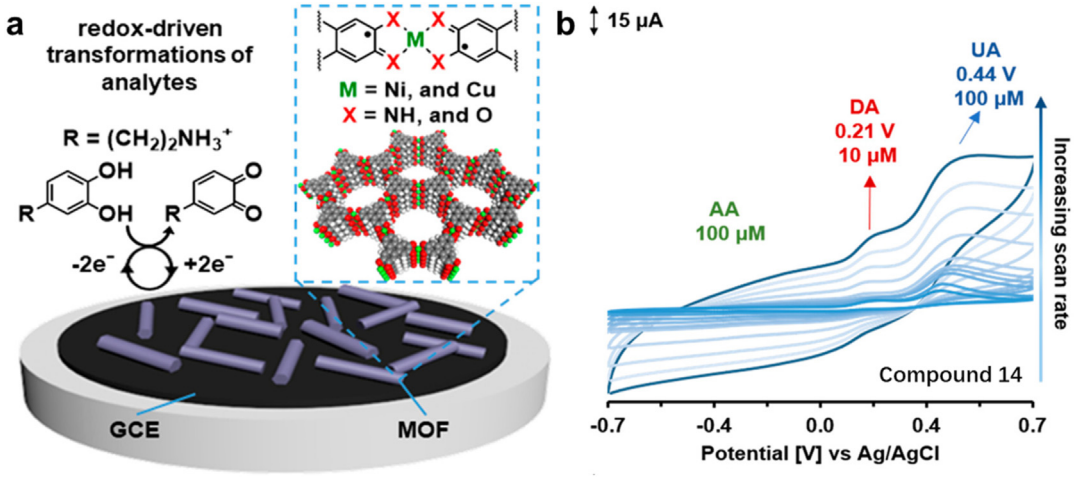

Fig. 8. (a) Schematic illustration of a 2D-cMOF structure and device mechanism. (b) CV curves of Compound 14 at different scan rates ranging from 5 to 1000 mV s^{-1} in PBS with three neurochemicals. Reprinted with permission from Ref. [62]. Copyright 2020, American Chemical Society.

Electrochemical sensors can be used to detect biomolecules within a corresponding electrochemical measurement window. The electrode materials should ideally exhibit infinitesimal or even no intrinsic activity for interferents. It is necessary to avoid masking the electrochemical signal generated by the analytes [64]. By ultrasonically treating and drop-casting 2D-cMOFs on a GCE, the Mirica group tested neurochemicals as organic probes. Dopamine (DA), ascorbic acid (AA), uric acid (UA), and serotonin (5-HT) were used to characterize the suitability of 2D-cMOF-based electrodes for voltammetric detection in 0.1 M PBS as the base electrolyte (Fig. 8b). Compound 13 and Compound 14 exhibited a large difference in response potential, with XPS showing only one type of oxidation state for Ni^{2+}. To detect AA, two-electron- and one-proton-mediated oxidation could occur on the GCE surface. The accumulation of oxidation products resulted in an irreversible voltammetric response. Unexpectedly, the cyclic stability of sensors was immensely improved by modifying the 2D-cMOFs. Since the oxidation of DA involved four steps, it responded with large differences on various electrode surfaces. Thus, the voltammetric response had been enhanced. In the UA assay, the unstable compound uric acid-4,5-diol was generated, which could be decomposed into various byproducts in the electrolyte, leading to electrode poisoning. Ni-based 2D-cMOFs exhibited slower electron transfer kinetics than Cu-based 2D-cMOFs, suggesting that the kinetics may have been influenced by the metal center. Because of the difference in redox potentials of Compound 14 for DA (0.33 V) and UA (0.47 V), selective detection was characterized in a 0.1 M PBS solution with a mixture of three neurochemicals. Through combining UA and AA, the DA peaks were easily resolved by the potential difference. The detection limit of DA was quantified at 63 ± 11 nM by differential pulse voltammetry. It was generally 36 and 11 times larger than that of an unmodified GCE electrode for DA (2.31 ± 0.79 μM) and 5-HT (0.45 ± 0.17 μM), respectively. The peak oxidation current increased linearly with analyte concentration (63 nM–200 μM). Stability testing of Compound 14 showed that the peak intensity of DA remained essentially constant for up to 100 cycles at 0.29 V.

3.2. Medicine

Excess of the reactive oxygen species H_2O_2 in the human body is associated with many diseases, including cardiac cancer, Parkinson's, and Alzheimer's. Thus, it is vital to develop high-performance H_2O_2 detection sensors [65]. Compound 20 has extremely high conductivity (2500 S cm^{-1}) [66]. Its sufficient active sites and competent electron transfer capability as a film can help construct ultra-sensitive electrochemical sensors. Compound 20 ultrathin films (16 nm thickness) with good crystallinity and strong microcrystalline orientation were prepared by Liu and co-workers (Fig. 9a) [67]. The results indicated that the outer surface of the Compound 20 film had just (001) crystallographic planes. They designed a Compound 20-based micro-biosensor device (Fig. 9b) to compare the H_2O_2 sensing property of Compound 20 films on their upper surface (US-Compound 20) and lower surface (BS-Compound 20). BS-Compound 20 and US-Compound 20 films all showed a very fast response to H_2O_2, reaching a steady state in only 4 s. The detection range was 0.0005–0.4 mM, with a limit of detection (LOD) of 0.08 μM and a sensitivity of 257 μA mM^{-1} cm^{-2}, which was better than many previously reported nanohybrid materials for non-enzymatic H_2O_2 sensors. The relative current response was 91.34% of the initial value after 14 days of cycling, demonstrating the good electrochemical cycling stability of the Compound 20 film. The interference immunity of BS-Compound 20 films was investigated in mixed systems (Fig. 9c) with biomolecules such as UA, DA, glucose (GLU), AA, and L-cysteine (L-CySH). The absence of significant amperometric current density changes demonstrated the films' good selectivity to H_2O_2. XPS patterns and DFT computing demonstrated that ts-Cu crystal defects (Cu bound to two S atoms) on BS-Compound 20 films are important reactive sites affecting the H_2O_2 sensing performance. Compared to the smooth upper surface (27.46% ts-Cu), the synaptic-like structure of the bottom surface (41.25% ts-Cu) had superior H_2O_2 sensing performance.

3.3. Pollutants

Besides human disease detection, electrochemical sensors can be used for environmental pollutant detection. Nitrite is a common pollutant found widely in agriculture, the food industry, and environmental protection endeavors. Because ecosystems and community health are severely damaged by the irresponsible utilization and disposal of nitrite, accurately detecting nitrite in daily life is vital [68,69]. Gu and co-workers synthesized nickel phthalocyanine-based 2D-cMOFs (Compound 9) by a solvothermal method (Figs. 10a and b) [70]. Compound 9 nanosheets exhibited superb nitrite sensing activity with a large linear range (0.01–11500 mM) and a 2.3 μM LOD (Fig. 10c). The materials still showed good nitrite selectivity with the introduction of successive interfering species at 0.9 V in 0.1 M PBS (Fig. 10d). The relative standard deviation (RSD) value (1.65%) for reproducibility showed the enormous potential of Compound 9 nanosheets for electroanalysis.

4. Summary and outlook

In conclusion, the high electrical conductivity, high surface area, and abundant catalytic active sites of MOFs can result in high activity for electrochemical catalysis (HER, ORR, OER, CRR, and NRR) and electrochemical sensors. In the last five years, exploring new structures for conductive MOFs to obtain unique physical and chemical properties has

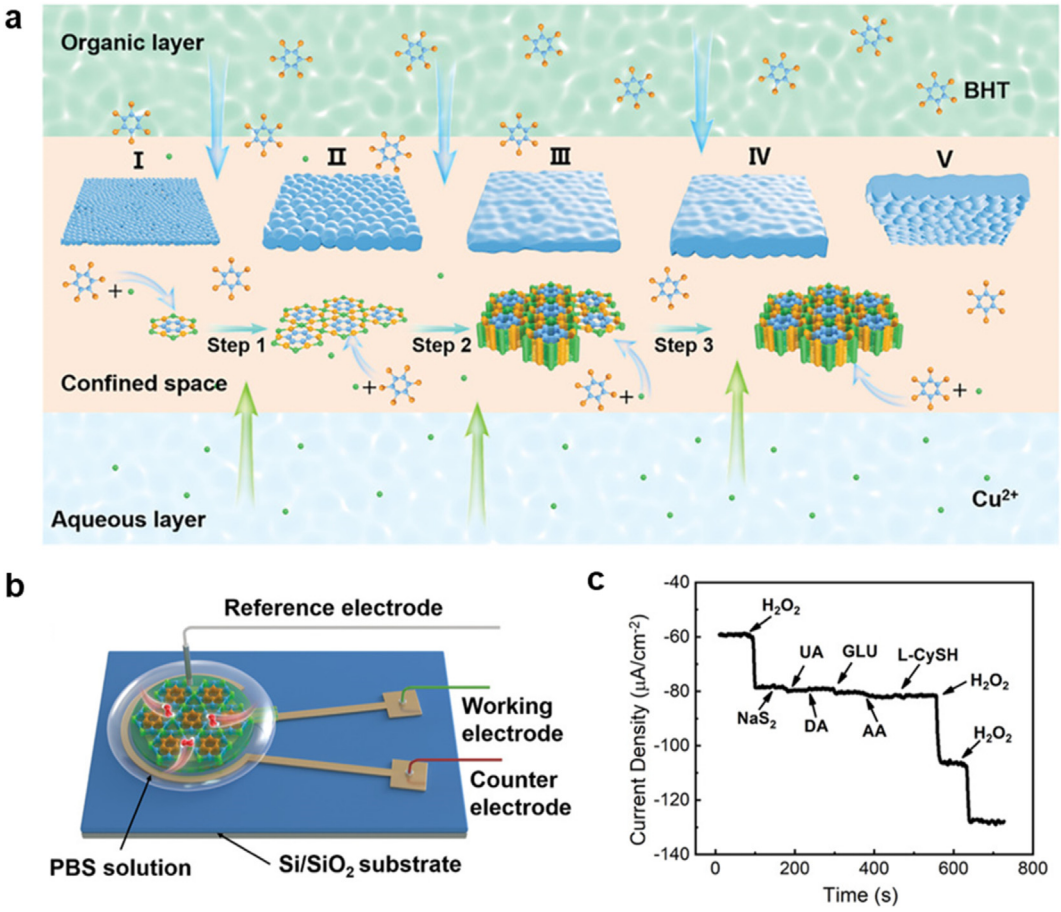

Fig. 9. (a) Illustration of Compound 20 film formation at the interface between water and organic matter. (b) Schematic of the Compound 20-based micro-biosensor device. (c) Amperometric response of the BS-Compound 20. Reprinted with permission from Ref. [67]. Copyright 2021, Wiley-VCH.

been an emerging research area. The overall advantages of conductive MOFs can be summarized as follows: (1) High specific areas and dense metal nodes create many open active sites in 2D-cMOFs, which enhance their electrocatalytic activity. (2) Excellent conductivity leads to efficient electron transfer throughout the catalyst and initiates charge transfer to the substrates or probe molecules. As a result, the intrinsic activity comes closer to the apparent activity, offering high sensitivity and accurate electrochemical signals. (3) Tunable components enable modulation of the electronic structure and adsorption capacity of active sites. With electrochemical properties superior to conventional MOFs, conductive MOFs hold significant promise for electrocatalysis and electrochemical sensors.

However, challenges remain for conductive MOFs in both fundamental research and application. Fundamental research includes the following obstacles: (1) The current ligands for constructing conductive MOFs are limited to THT, HITP, etc., the organic synthesis of which requires significant labor. Affordable and commercially available ligands need to be applied in conductive MOFs to promote their broad-spectrum use. (2) The crystallinity of conductive MOFs is difficult to maintain during the electrocatalytic process. High crystallinity can improve a material's electrical conductivity and charge capacity, which is beneficial for the study of structure–property relationships. However, the presence of defects usually determines the number of catalytic sites and thus affects the material's catalytic performance. A new synthesis or modification method must be developed to modulate crystallinity and precisely construct defects to improve catalytic performance. (3) The catalytic activity explored in existing studies mainly relies on a single type of metal center. Conductive MOFs containing intrinsic mixed metals may show unpredictable effects compared to those bearing single metals. Furthermore, the study of the catalytic activity of specific functional groups in organic ligands is still limited.

In the application field remain the following problems: (1) Existing studies have not deeply explored the connection between conductivity and catalytic activity, which requires that a substantial number of samples in a given system be investigated. (2) The electrochemical processes occurring in the CRR are complicated, and the reactions usually generate a wide range of products. Electrocatalysts' selectivity for reaction products needs to be investigated at the molecular level. (3) The selectivity of conductive MOFs as electrochemical sensors has not yet been demonstrated, and the catalytic effect of different targets has not been studied in depth. The correlations between their conductivity and their sensitivity and selectivity need to be fully addressed. (4) The reaction mechanism still needs to be elucidated, including the correlations between different probe types and materials, organic and inorganic probes, different charge probes, and materials with different dimensions and morphological size, surface functional groups, heteroatom content, and metal centers.

Since researchers still have only a vague understanding of the mechanism and the "structure–property relationship" in conductive MOFs for electrocatalysis and electrochemical sensors, a new approach is required. In our view, the dimension of the current conductive MOFs limits rational design and further creativity. Beyond 2D frameworks, the dimension of the conductive complex could also be extended to three dimensions (3D) or zero dimensions (0D) to explore high-performance candidates for electrocatalysis and sensors. Although there are plenty of reports about 3D conductive MOFs (3D-cMOFs) [71–77], their advantages have not been emphasized in comparison with 2D frameworks. Because 2D-cMOFs possess the π-conjugated stacked structure, they exhibit excellent electrical conductivity. However, due to the limited

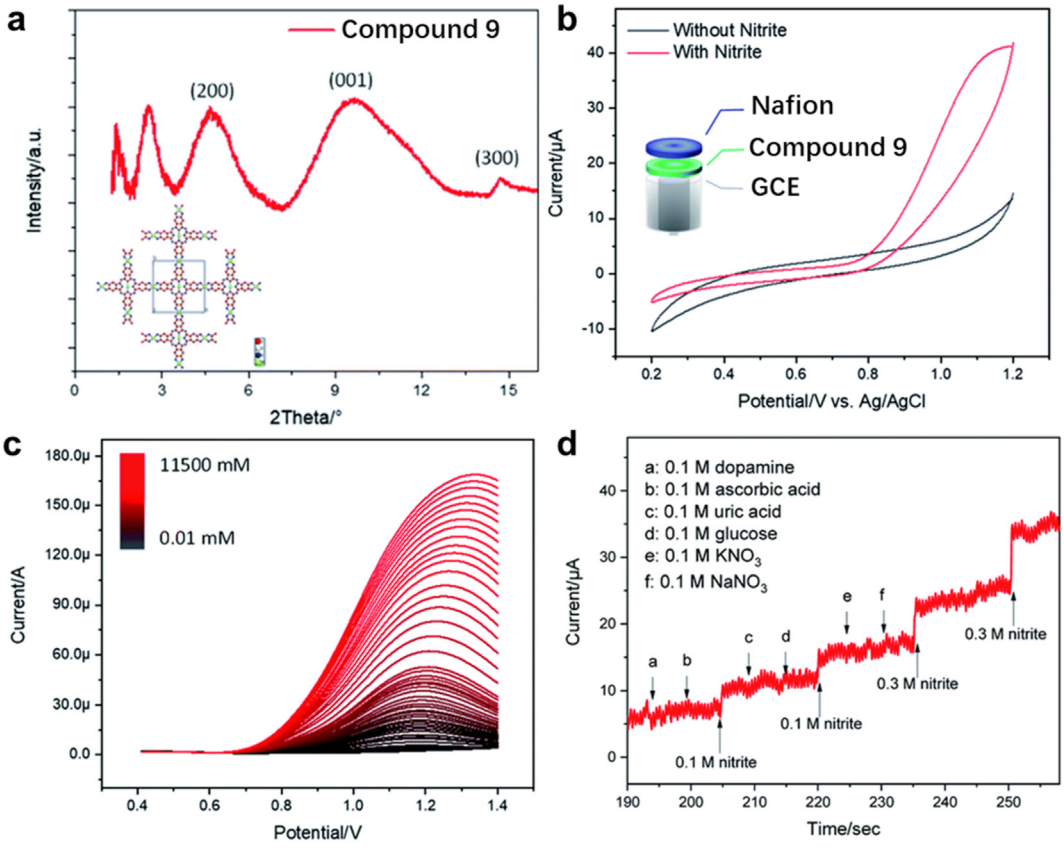

Fig. 10. (a) The PXRD pattern and structure of Compound 9. (b) CV curves of Compound 9 electrode. (c) DPV curves of Compound 9 electrode (0.01–11500 mM). (d) Amperometry curve of Compound 9 electrode at 0.9 V. Reprinted with permission from Ref. [70]. Copyright 2021, Royal Society of Chemistry.

exposure of active centers and weak electronic interactions, some 2D-cMOFs have poor catalytic activity. In contrast, 3D structures not only expose more active sites but also effectively prohibit aggregation.

Alternatively, a 0D structure can be more accurately tuned on a molecular level, and the reaction pathway can be elucidated. However, the investigation of discrete porous materials for electrocatalysis is relatively rare. For example, metallomacrocycles, multinuclear metal complexes, and molecular cages can be applied as electrodes, electrocatalysts, and electric sensors. As a sibling of the MOF, the porous coordination cage (PCC), which exhibits a discrete 0D structure with multiple tunable 3D cavities, permits fine tuning of the cavity function, cavity size, and redox species, enabling one to study the relationship between the cage structure

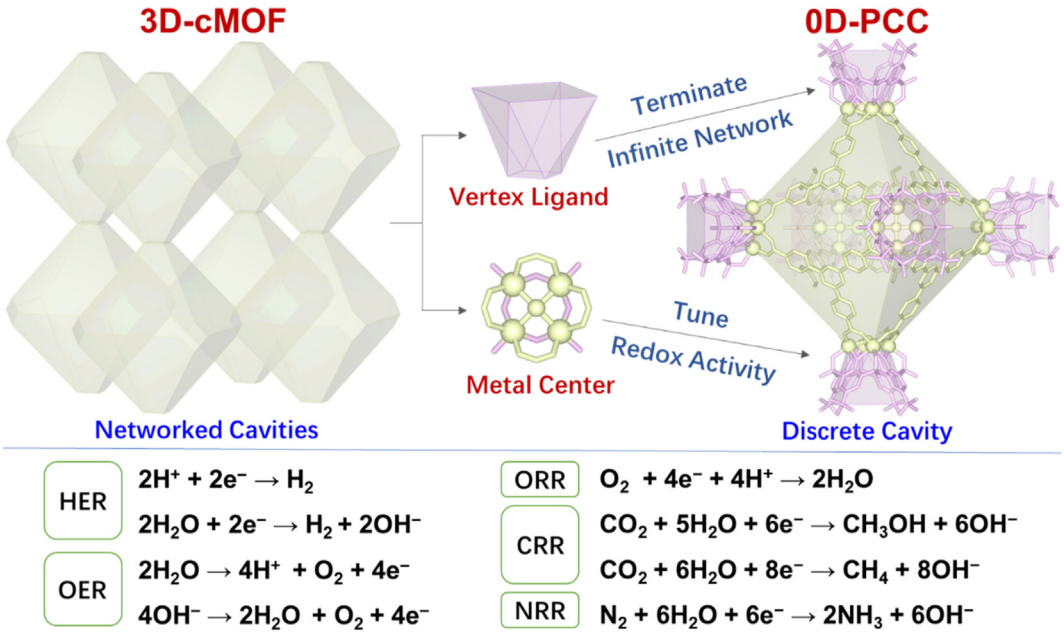

Scheme 1. 0D PCCs inherit 3D cavities and tunable redox activity from 3D-cMOFs for electrocatalysis.

and the electrochemical performance [78–83]. PCCs can be viewed as a "top-down" version of 3D-cMOFs, inheriting merits such as high redox activity and high surface area from the networks and thus holding out great promise for energy storage and electrochemical reaction purposes (Scheme 1). It is expected that the redox metal centers of PCCs could serve as active sites for catalysis, and the pores/cavities of PCCs could allow for deep research on the structure–property relationship. We envision a judiciously designed PCC being validated as a potential flexible energy storage and electrocatalytic material that would pave the way for designing high-performance energy storage devices by taking full advantage of the large pool of metal–organic complexes.

As a result, although the current research on conductive MOFs in the field of electrocatalysis and sensors is still in the initial exploration stage, the fascinating structures and abundant properties of coordination chemistry offer broad development prospects that could have far-reaching significance for human society.

Author contributions

Hai-Long Jiang and Yu Fang conceived the idea. Kangkai Liu wrote the manuscript and did the figure work. Zheng Meng provided advice on the context and did language editing. Yu Fang edited the cartoons and tables. Hai-Long Jiang supervised the project and provided revision. All authors participated in manuscript discussions and revisions.

Competing financial interests

The authors declare that they have no known competing financial interests or personal relationships that could have appeared to influence the work reported in this paper.

Acknowledgments

We thank the National Key Research and Development Program of China (2021YFA1500400), NSFC (21501133, U22A20401, and 22161142001), and China Hunan Provincial Science & Technology Department (2020RC3020; 2021JJ20021) for their support.

References

[1] Y. Li, Z. Dong, L. Jiao, Multifunctional transition metal-based phosphides in energy-related electrocatalysis, Adv. Energy Mater. 10 (2019) 1902104.
[2] X. Ma, H. Liu, W. Yang, G. Mao, L. Zheng, H.-L. Jiang, Modulating coordination environment of single-atom catalysts and their proximity to photosensitive units for boosting MOF photocatalysis, J. Am. Chem. Soc. 143 (2021) 12220–12229.
[3] Z. Chen, H. Qing, K. Zhou, D. Sun, R. Wu, Metal-organic framework-derived nanocomposites for electrocatalytic hydrogen evolution reaction, Prog. Mater. Sci. 108 (2020) 100618.
[4] Y. Wu, Y. Li, J. Gao, Q. Zhang, Recent advances in vacancy engineering of metal-organic frameworks and their derivatives for electrocatalysis, Sustain. Mater. 1 (2021) 66–87.
[5] H.-F. Wang, L. Chen, H. Pang, S. Kaskel, Q. Xu, MOF-derived electrocatalysts for oxygen reduction, oxygen evolution, and hydrogen evolution reactions, Chem. Soc. Rev. 49 (2020) 1414–1448.
[6] Q. Wang, Y. Lei, D. Wang, Y. Li, Defect engineering in earth-abundant electrocatalysts for CO_2 and N_2 reduction, Energy Environ. Sci. 12 (2019) 1730–1750.
[7] J. Min, J.R. Sempionatto, H. Teymourian, J. Wang, W. Gao, Wearable electrochemical biosensors in north America, Biosens. Bioelectron. 172 (2021) 112750.
[8] S. Kumar, S.D. Bukkitgar, S. Singh, Pratibha, V. Singh, K.R. Reddy, N.P. Shetti, C. Venkata Reddy, V. Sadhu, S. Naveen, Electrochemical sensors and biosensors based on graphene functionalized with metal oxide nanostructures for healthcare applications, ChemistrySelect 4 (2019) 5322–5337.
[9] T. Xiao, J. Huang, D. Wang, T. Meng, X. Yang, Au and Au-based nanomaterials: synthesis and recent progress in electrochemical sensor applications, Talanta 206 (2020) 120210.
[10] D. Zhu, M. Qiao, J. Liu, T. Tao, C. Guo, Engineering pristine 2D metal-organic framework nanosheets for electrocatalysis, J. Mater. Chem. A 8 (2020) 8143–8170.
[11] L. Jiao, J. Wang, H.-L. Jiang, Microenvironment modulation in metal–organic framework-based catalysis, Acc. Mater. Res. 2 (2021) 327–339.
[12] L. Jiao, W. Yang, G. Wan, R. Zhang, X. Zheng, H. Zhou, S.-H. Yu, H.-L. Jiang, Single-atom electrocatalysts from multivariate metal-organic frameworks for highly selective reduction of CO_2 at low pressures, Angew. Chem. Int. Ed. 59 (2020) 20589–20595.
[13] Z. Xin, Y.-R. Wang, Y. Chen, W.-L. Li, L.-Z. Dong, Y.-Q. Lan, Metallocene implanted metalloporphyrin organic framework for highly selective CO_2 electroreduction, Nano Energy 67 (2020) 104233.
[14] G.T. Chandran, X. Li, A. Ogata, R.M. Penner, Electrically transduced sensors based on nanomaterials (2012-2016), Anal. Chem. 89 (2017) 249–275.
[15] E. Peltola, S. Sainio, K.B. Holt, T. Palomäki, J. Koskinen, T. Laurila, Electrochemical fouling of dopamine and recovery of carbon electrodes, Anal. Chem. 90 (2018) 1408–1416.
[16] T. Chen, F. Wang, S. Cao, Y. Bai, S. Zheng, W. Li, S. Zhang, S.-X. Hu, H. Pang, In situ synthesis of MOF-74 family for high areal energy density of aqueous nickel-zinc batteries, Adv. Mater. 34 (2022) e2201779.
[17] P. Geng, L. Wang, M. Du, Y. Bai, W. Li, Y. Liu, S. Chen, P. Braunstein, Q. Xu, H. Pang, MIL-96-Al for Li-S batteries: shape or size? Adv. Mater. 34 (2022) e2107836.
[18] X. Guo, H. Xu, W. Li, Y. Liu, Y. Shi, Q. Li, H. Pang, Embedding atomically dispersed iron sites in nitrogen-doped carbon frameworks-wrapped silicon suboxide for superior lithium storage, Adv. Sci. 10 (2023) e2206084.
[19] L. Ding, H. Hong, L. Xiao, Q. Hu, Y. Zuo, N. Hao, J. Wei, K. Wang, Nanoparticles-doped induced defective ZIF-8 as the novel cathodic luminophore for fabricating high-performance electrochemiluminescence aptasensor for detection of omethoate, Biosens. Bioelectron. 192 (2021) 113492.
[20] Y. Cong, S. Huang, Y. Mei, T.-T. Li, Metal-organic frameworks-derived self-supported carbon-based composites for electrocatalytic water splitting, Chem. Eur. J. 27 (2021) 15866–15888.
[21] C.H. Ahn, N.G. Deshpande, H.S. Lee, H.K. Cho, Atomically controllable in-situ electrochemical treatment of metal-organic-framework-derived cobalt-embedded carbon composites for highly efficient electrocatalytic oxygen evolution, Appl. Surf. Sci. 554 (2021) 149651.
[22] L. Sun, M.G. Campbell, M. Dinca, Electrically conductive porous metal-organic frameworks, Angew. Chem. Int. Ed. 55 (2016) 3566–3579.
[23] L.S. Xie, G. Skorupskii, M. Dincă, Electrically conductive metal-organic frameworks, Chem. Rev. 120 (2020) 8536–8580.
[24] G. Skorupskii, B.A. Trump, T.W. Kasel, C.M. Brown, C.H. Hendon, M. Dincă, Efficient and tunable one-dimensional charge transport in layered lanthanide metal-organic frameworks, Nat. Chem. 12 (2020) 131–136.
[25] T. He, X.-J. Kong, J.-R. Li, Chemically stable metal-organic frameworks: rational construction and application expansion, Acc. Chem. Res. 54 (2021) 3083–3094.
[26] J. Liu, X. Song, T. Zhang, S. Liu, H. Wen, L. Chen, 2D Conductive metal-organic frameworks: an emerging platform for electrochemical energy storage, Angew. Chem. Int. Ed. 60 (2021) 5612–5624.
[27] H. Yu, Y. Jing, C.-F. Du, J. Wang, Tuning the reversible chemisorption of hydroxyl ions to promote the electrocatalysis on ultrathin metal-organic framework nanosheets, J. Energy Chem. 65 (2022) 71–77.
[28] W. Zheng, L.Y.S. Lee, Metal–organic frameworks for electrocatalysis: catalyst or precatalyst? ACS Energy Lett. 6 (2021) 2838–2843.
[29] L. Jiao, G. Wan, R. Zhang, H. Zhou, S.-H. Yu, H.-L. Jiang, From metal-organic frameworks to single-atom Fe implanted N-doped porous carbons: efficient oxygen reduction in both alkaline and acidic media, Angew. Chem. Int. Ed. 57 (2018) 8525–8529.
[30] T. Kambe, R. Sakamoto, K. Hoshiko, K. Takada, M. Miyachi, J.-H. Ryu, S. Sasaki, J. Kim, K. Nakazato, M. Takata, H. Nishihara, π-conjugated nickel bis(dithiolene) complex nanosheet, J. Am. Chem. Soc. 135 (2013) 2462–2465.
[31] R. Dong, M. Pfeffermann, H. Liang, Z. Zheng, X. Zhu, J. Zhang, X. Feng, Large-area, free-standing, two-dimensional supramolecular polymer single-layer sheets for highly efficient electrocatalytic hydrogen evolution, Angew. Chem. Int. Ed. 54 (2015) 12058–12063.
[32] R. Dong, Z. Zheng, D.C. Tranca, J. Zhang, N. Chandrasekhar, S. Liu, X. Zhuang, G. Seifert, X. Feng, Immobilizing molecular metal dithiolene-diamine complexes on 2D metal-organic frameworks for electrocatalytic H_2 production, Chem. Eur. J. 23 (2017) 2255–2260.
[33] X. Sun, K.-H. Wu, R. Sakamoto, T. Kusamoto, H. Maeda, X. Ni, W. Jiang, F. Liu, S. Sasaki, H. Masunaga, H. Nishihara, Bis(aminothiolato)nickel nanosheet as a redox switch for conductivity and an electrocatalyst for the hydrogen evolution reaction, Chem. Sci. 8 (2017) 8078–8085.
[34] D. Sheberla, L. Sun, M.A. Blood-Forsythe, S.l. Er, C.R. Wade, C.K. Brozek, A. Aspuru-Guzik, M. Dincă, High electrical conductivity in Ni_3(2,3,6,7,10,11-hexaiminotriphenylene)$_2$, a semiconducting metal–organic graphene analogue, J. Am. Chem. Soc. 136 (2014) 8859–8862.
[35] H. Huang, Y. Zhao, Y. Bai, F. Li, Y. Zhang, Y. Chen, Conductive metal-organic frameworks with extra metallic sites as an efficient electrocatalyst for the hydrogen evolution reaction, Adv. Sci. 7 (2020) 2000012.
[36] Z. Xue, K. Liu, Q. Liu, Y. Li, M. Li, C.-Y. Su, N. Ogiwara, H. Kobayashi, H. Kitagawa, M. Liu, G. Li, Missing-linker metal-organic frameworks for oxygen evolution reaction, Nat. Commun. 10 (2019) 5048.
[37] X. Fang, L. Jiao, R. Zhang, H.-L. Jiang, Porphyrinic metal-organic framework-templated Fe-Ni-P/reduced graphene oxide for efficient electrocatalytic oxygen evolution, ACS Appl. Mater. Interfaces 9 (2017) 23852–23858.
[38] H. Jia, Y. Yao, J. Zhao, Y. Gao, Z. Luo, P. Du, A novel two-dimensional nickel phthalocyanine-based metal–organic framework for highly efficient water oxidation catalysis, J. Mater. Chem. A 6 (2018) 1188–1195.
[39] J. Li, P. Liu, J. Mao, J. Yan, W. Song, Two-dimensional conductive metal–organic frameworks with dual metal sites toward the electrochemical oxygen evolution reaction, J. Mater. Chem. A 9 (2021) 1623–1629.
[40] J. Li, P. Liu, J. Mao, J. Yan, W. Song, Structural and electronic modulation of conductive MOFs for efficient oxygen evolution reaction electrocatalysis, J. Mater. Chem. A 9 (2021) 11248–11254.

[41] C. Li, L. Shi, L. Zhang, P. Chen, J. Zhu, X. Wang, Y. Fu, Ultrathin two-dimensional π–d conjugated coordination polymer Co_3(hexaaminobenzene)$_2$ nanosheets for highly efficient oxygen evolution, J. Mater. Chem. A 8 (2020) 369–379.

[42] Z. Liang, H. Guo, G. Zhou, K. Guo, B. Wang, H. Lei, W. Zhang, H. Zheng, U.-P. Apfel, R. Cao, Metal-organic-framework-supported molecular electrocatalysis for the oxygen reduction reaction, Angew. Chem. Int. Ed. 60 (2021) 8472–8476.

[43] E.M. Miner, T. Fukushima, D. Sheberla, L. Sun, Y. Surendranath, M. Dincă, Electrochemical oxygen reduction catalysed by Ni_3(hexaiminotriphenylene)$_2$, Nat. Commun. 7 (2016) 10942.

[44] X.-H. Liu, W.-L. Hu, W.-J. Jiang, Y.-W. Yang, S. Niu, B. Sun, J. Wu, J.-S. Hu, Well-defined metal–O_6 in metal–catecholates as a novel active site for oxygen electroreduction, ACS Appl. Mater. Inter. 9 (2017) 28473–28477.

[45] M. Hmadeh, Z. Lu, Z. Liu, F. Gándara, H. Furukawa, S. Wan, V. Augustyn, R. Chang, L. Liao, F. Zhou, E. Perre, V. Ozolins, K. Suenaga, X. Duan, B. Dunn, Y. Yamamto, O. Terasaki, O.M. Yaghi, New porous crystals of extended metal-catecholates, Chem. Mater. 24 (2012) 3511–3513.

[46] H. Yoon, S. Lee, S. Oh, H. Park, S. Choi, M. Oh, Synthesis of bimetallic conductive 2D metal–organic framework (Co_xNi_y-CAT) and its mass production: enhanced electrochemical oxygen reduction activity, Small 15 (2019) e1805232.

[47] L. Wang, W. Chen, D. Zhang, Y. Du, R. Amal, S. Qiao, J. Wu, Z. Yin, Surface strategies for catalytic CO_2 reduction: from two-dimensional materials to nanoclusters to single atoms, Chem. Soc. Rev. 48 (2019) 5310–5349.

[48] H. Zhong, M. Ghorbani-Asl, K.H. Ly, J. Zhang, J. Ge, M. Wang, Z. Liao, D. Makarov, E. Zschech, E. Brunner, I.M. Weidinger, J. Zhang, A.V. Krasheninnikov, S. Kaskel, R. Dong, X. Feng, Synergistic electroreduction of carbon dioxide to carbon monoxide on bimetallic layered conjugated metal-organic frameworks, Nat. Commun. 11 (2020) 1409.

[49] Z. Meng, J. Luo, W. Li, K.A. Mirica, Hierarchical tuning of the performance of electrochemical carbon dioxide reduction using conductive two-dimensional metallophthalocyanine based metal-organic frameworks, J. Am. Chem. Soc. 142 (2020) 21656–21669.

[50] X.F. Qiu, H.L. Zhu, J.R. Huang, P.Q. Liao, X.M. Chen, Highly selective CO_2 electroreduction to C_2H_4 using a metal-organic framework with dual active sites, J. Am. Chem. Soc. 143 (2021) 7242–7246.

[51] X. Liu, H. Yang, J. He, H. Liu, L. Song, L. Li, J. Luo, Highly active, durable ultrathin $MoTe_2$ layers for the electroreduction of CO_2 to CH_4, Small 14 (2018) e1704049.

[52] J. Kim, W. Choi, J.W. Park, C. Kim, M. Kim, H. Song, Branched copper oxide nanoparticles induce highly selective ethylene production by electrochemical carbon dioxide reduction, J. Am. Chem. Soc. 141 (2019) 6986–6994.

[53] Y. Zhang, L.-Z. Dong, S. Li, X. Huang, J.-N. Chang, J.-H. Wang, J. Zhou, S.-L. Li, Y.-Q. Lan, Coordination environment dependent selectivity of single-site-Cu enriched crystalline porous catalysts in CO_2 reduction to CH_4, Nat. Commun. 12 (2021) 6390.

[54] J. Liang, Q. Liu, A.A. Alshehri, X. Sun, Recent advances in nanostructured heterogeneous catalysts for N-cycle electrocatalysis, Nano Res. Energy 1 (2022) e9120010.

[55] R. Zhang, L. Jiao, W. Yang, G. Wan, H.-L. Jiang, Single-atom catalysts templated by metal–organic frameworks for electrochemical nitrogen reduction, J. Mater. Chem. A 7 (2019) 26371–26377.

[56] J. Zhao, Z. Chen, Single Mo atom supported on defective boron nitride monolayer as an efficient electrocatalyst for nitrogen fixation: a computational study, J. Am. Chem. Soc. 139 (2017) 12480–12487.

[57] C. Ling, X. Niu, Q. Li, A. Du, J. Wang, Metal-free single atom catalyst for N_2 fixation driven by visible light, J. Am. Chem. Soc. 140 (2018) 14161–14168.

[58] Q. Cui, G. Qin, W. Wang, G.K.R.A. Du, Q. Sun, Mo-based 2D MOF as a highly efficient electrocatalyst for reduction of N_2 to NH_3: a density functional theory study, J. Mater. Chem. A 7 (2019) 14510–14518.

[59] W. Xiong, X. Cheng, T. Wang, Y. Luo, J. Feng, S. Lu, A.M. Asiri, W. Li, Z. Jiang, X. Sun, Co_3(hexahydroxytriphenylene)$_2$: a conductive metal–organic framework for ambient electrocatalytic N_2 reduction to NH_3, Nano Res. 13 (2020) 1008–1012.

[60] L. Jiao, R. Zhang, G. Wan, W. Yang, X. Wan, H. Zhou, J. Shui, S.-H. Yu, H.-L. Jiang, Nanocasting SiO_2 into metal-organic frameworks imparts dual protection to high-loading Fe single-atom electrocatalysts, Nat. Commun. 11 (2020) 2831.

[61] A.J. Bandodkar, I. Jeerapan, J. Wang, Wearable chemical sensors: present challenges and future prospects, ACS Sens. 1 (2016) 464–482.

[62] M. Ko, L. Mendecki, A.M. Eagleton, C.G. Durbin, R.M. Stolz, Z. Meng, K.A. Mirica, Employing conductive metal-organic frameworks for voltammetric detection of neurochemicals, J. Am. Chem. Soc. 142 (2020) 11717–11733.

[63] K. Wijeratne, U. Ail, R. Brooke, M. Vagin, X. Liu, M. Fahlman, X. Crispin, Bulk electronic transport impacts on electron transfer at conducting polymer electrode-electrolyte interfaces, Proc. Natl. Acad. Sci. U.S.A. 115 (2018) 11899–11904.

[64] Z. Qiu, T. Yang, R. Gao, G. Jie, W. Hou, An electrochemical ratiometric sensor based on 2D MOF nanosheet/Au/polyxanthurenic acid composite for detection of dopamine, J. Electroanal. Chem. 835 (2019) 123–129.

[65] B. Patella, R. Inguanta, S. Piazza, C. Sunseri, A nanostructured sensor of hydrogen peroxide, Sens. Actuators B Chem. 245 (2017) 44–54.

[66] X. Huang, S. Zhang, L. Liu, L. Yu, G. Chen, W. Xu, D. Zhu, Superconductivity in a copper(II)-based coordination polymer with perfect kagome structure, Angew. Chem. Int. Ed. 57 (2018) 146–150.

[67] X. Chen, J. Dong, K. Chi, L. Wang, F. Xiao, S. Wang, Y. Zhao, Y. Liu, Electrically conductive metal–organic framework thin film-based on-chip micro-biosensor: a platform to unravel surface morphology-dependent biosensing, Adv. Funct. Mater. 31 (2021) 2102855.

[68] C. Hong, P. Zhang, K. Lu, Y. Ji, S. He, D. Liu, N. Jia, A dual-signal electrochemiluminescence immunosensor for high-sensitivity detection of acute myocardial infarction biomarker, Biosens. Bioelectron. 194 (2021) 113591.

[69] M. Annalakshmi, S. Kumaravel, S.-M. Chen, P. Balasubramanian, T.S.T. Balamurugan, A straightforward ultrasonic-assisted synthesis of zinc sulfide for supersensitive detection of carcinogenic nitrite ions in water samples, Sens. Actuators B Chem. 305 (2020) 127387.

[70] S. Lu, H. Jia, M. Hummel, Y. Wu, K. Wang, X. Qi, Z. Gu, Two-dimensional conductive phthalocyanine-based metal-organic frameworks for electrochemical nitrite sensing, RSC Adv. 11 (2021) 4472–4477.

[71] I. Hod, M.D. Sampson, P. Deria, C.P. Kubiak, O.K. Farha, J.T. Hupp, Fe-porphyrin-based metal–organic framework films as high-surface concentration, heterogeneous catalysts for electrochemical reduction of CO_2, ACS Catal. 5 (2015) 6302–6309.

[72] Z. Xue, K. Liu, Q. Liu, Y. Li, M. Li, C.-Y. Su, N. Ogiwara, H. Kobayashi, H. Kitagawa, M. Liu, G. Li, Missing-linker metal-organic frameworks for oxygen evolution reaction, Nat. Commun. 10 (2019) 5048.

[73] X. Han, X. Ling, Y. Wang, T. Ma, C. Zhong, W. Hu, Y. Deng, Generation of nanoparticle, atomic-cluster, and single-atom cobalt catalysts from zeolitic imidazole frameworks by spatial isolation and their use in zinc-air batteries, Angew. Chem. Int. Ed. 58 (2019) 5359–5364.

[74] P. He, X.Y. Yu, X.W. Lou, Carbon-incorporated nickel-cobalt mixed metal phosphide nanoboxes with enhanced electrocatalytic activity for oxygen evolution, Angew. Chem. Int. Ed. 56 (2017) 3897–3900.

[75] Z. Liang, H. Guo, G. Zhou, K. Guo, B. Wang, H. Lei, W. Zhang, H. Zheng, U.-P. Apfel, R. Cao, Metal-organic-framework-supported molecular electrocatalysis for the oxygen reduction reaction, Angew. Chem. Int. Ed. 60 (2021) 8472–8476.

[76] Y. Sun, Z. Xue, Q. Liu, Y. Jia, Y. Li, K. Liu, Y. Lin, M. Liu, G. Li, C.-Y. Su, Modulating electronic structure of metal-organic frameworks by introducing atomically dispersed Ru for efficient hydrogen evolution, Nat. Commun. 12 (2021) 1369.

[77] W. Zhang, Z.-Y. Wu, H.-L. Jiang, S.-H. Yu, Nanowire-directed templating synthesis of metal-organic framework nanofibers and their derived porous doped carbon nanofibers for enhanced electrocatalysis, J. Am. Chem. Soc. 136 (2014) 14385–14388.

[78] C. Zhu, H. Tang, K. Yang, Y. Fang, K.-Y. Wang, Z. Xiao, X. Wu, Y. Li, J.A. Powell, H.-C. Zhou, Homochiral dodecanuclear lanthanide "cage in cage" for enantioselective separation, J. Am. Chem. Soc. 143 (2021) 12560–12566.

[79] Y. Liang, Y. Fang, Y. Cui, H. Zhou, A stable biocompatible porous coordination cage promotes in vivo liver tumor inhibition, Nano Res. 14 (2021) 3407–3415.

[80] Y. Fang, X. Lian, Y. Huang, G. Fu, Z. Xiao, Q. Wang, B. Nan, J.-P. Pellois, H.-C. Zhou, Investigating subcellular compartment targeting effect of porous coordination cages for enhancing cancer nanotherapy, Small 14 (2018) e1802709.

[81] Y. Fang, T. Murase, S. Sato, M. Fujita, Noncovalent tailoring of the binding pocket of self-assembled cages by remote bulky ancillary groups, J. Am. Chem. Soc. 135 (2013) 613–615.

[82] Y. Fang, Z. Xiao, A. Kirchon, J. Li, F. Jin, T. Togo, L. Zhang, C. Zhu, H.-C. Zhou, Bimolecular proximity of a ruthenium complex and methylene blue within an anionic porous coordination cage for enhancing photocatalytic activity, Chem. Sci. 10 (2019) 3529–3534.

[83] Y. Fang, Z. Xiao, J. Li, C. Lollar, L. Liu, X. Lian, S. Yuan, S. Banerjee, P. Zhang, H.-C. Zhou, Formation of a highly reactive cobalt nanocluster crystal within a highly negatively charged porous coordination cage, Angew. Chem. Int. Ed. 57 (2018) 5283–5287.